A multispectral vision system to evaluate enzymatic browning in fresh-cut apple slices

Loredana Lunadei , Pamela Galleguillos , Belén Diezma , Lourdes Lleó , Luis Ruiz-Garcia

Laboratorio de Propiedades Físicas y Tecnologías Avanzadas en Agroalimentación, Departamento de Ingeniería Rural, E.T.S.I. Agrónomos, Universidad Politécnica de Madrid, Av. Complutense s/n, Ciudad Universitaria, 28040 Madrid, Spain

Centro de Estudios Postcosecha CEPOC, Departamento de Producción Agrícola, Facultad de Ciencias Agronómicas, Universidad de Chile, Chile

Departamento de Ciencia y Tecnologías Aplicadas a la Ingeniería Técnica Agrícola, E.U.I.T. Agrícolas 5, Universidad Politécnica de Madrid, Av. Complutense s/n, Ciudad Universitaria, 28040 Madrid, Spain

Keywords:
Fresh-cut apples
Enzymatic browning
CIE $L^*a^*b^*$ color space
Multispectral images
Image analysis

A B S T R A C T

The main objective of this study was to develop a vision system that is able to classify fresh-cut apple slices according to the development of enzymatic browning. The experiment was carried out on 'Granny Smith' apple slices stored at 7.5 °C for 9 days ($n = 120$). Twenty-four samples were analyzed per day: at zero time and after storage for 1, 3, 7 and 9 days, which corresponds to treatments t_0, t_1, t_3, t_7 and t_9 respectively. Multispectral images were acquired from the samples by employing a 3-CCD camera centered at the infrared (IR, 800 nm), red (R, 680 nm) and blue (B, 450 nm) wavelengths. Apple slices were evaluated visually according to a visual color scale of 1–5 (where 1 corresponds to *fresh samples without any browning* and 5 to *samples with severe discoloration*), to obtain a sensory evaluation index (I_{SE}) for each sample. Finally, for each sample and for each treatment, visible (VIS) relative reflectance spectra (360–740 nm) were obtained. In order to identify the most related wavelengths to enzymatic browning evolution, unsupervised pattern recognition analysis of VIS reflectance spectra was performed by principal components analysis (PCA) on the autoscaled data. Maximum loading values corresponding to the B and R areas were observed. Therefore, a classification procedure was applied to the relative histograms of the following monochromatic images (virtual images), which were computed pixel by pixel: (R − B)/(R + B), R − B and B/R. In all cases, a non-supervised classification procedure was able to generate three image-based *browning reference classes* (BRC): Cluster A (corresponding to the t_0 samples), Cluster B (t_1 and t_3 samples) and Cluster C (t_7 and t_9 samples). An internal and an external validation ($n = 120$) were carried out, and the best classifications were obtained with the (R − B)/(R + B) and B/R image histograms (internal validation: 99.2% of samples correctly classified for both virtual images; external validation: 84% with (R − B)/(R + B) and 81% with B/R). The camera classification was evaluated according to the colorimetric measurements, which were usually utilized to evaluate enzymatic browning development (CIE $L^*a^*b^*$ color parameters and browning index, BI) and according to I_{SE}. For both validation phases a^*, b^*, BI and I_{SE} increased while L^* values decreased with image-based class number, thereby reflecting their browning state.

1. Introduction

The act of cutting fresh produce invariably stimulates a range of degradative changes, which present additional challenges to the fresh-cut industry to maintain quality for an acceptable marketing period. An important factor causing loss of quality in much produce is the development of browning on cut surfaces. Browning has a significant impact on the quality of apples and their products because it results in changes in the appearance and organoleptic properties of the food, which can affect market value and, in some cases, result in exclusion of the food product from certain markets (Pristijono et al., 2006). Browning is generally considered to be caused by a range of endogenous phenolic compounds containing an *o*-dihydroxy group that is oxidized to the corresponding *o*-quinones in the presence of oxygen by an oxidizing enzyme (in particular, polypheloloxidase (PPO)), with subsequent reactions leading to the formation of brown, black or red pigments (melanins) (Robards et al., 1999). The control of cut-surface browning is critical for maintaining the quality and safety of fresh-cut produce. The use of anti-browning agents based on citric or ascorbic acid, together with modified atmosphere packaging and low-temperature storage increases the shelf life of fresh-cut fruit (Baldwin et al., 1996).

Traditionally, enzymatic browning has been quantified using browning indicators through a biochemical index. For example,

using polyphenol oxidase activity (Osanai et al., 2003; Hosoda et al., 2005), or physical indicators such as surface color have been used (Lambrecht, 1995; Kang et al., 2004). In the case of physical indicators based on color, CIE $L^*a^*b^*$ color space has been the most extensively used color model due to the uniform distribution of colors and because it is very close to the human perception of color (Yam and Papadakis, 2004). Based on CIE $L^*a^*b^*$ coordinates, especially on the L^* value, or on CIE *XYZ* color space (a color model strongly related to the *Lab*), browning indicators in fruit have been developed (Pristijono et al., 2006; Lu et al., 2007). A browning index (BI), defined as brown color purity, is one of the most common indicators of browning in sugar containing food products (Buera et al., 1986). In order to carry out a detailed characterization of the color of a food item, and thus to more precisely evaluate its quality, it is necessary to know the color value of each point of its surface (León et al., 2006). However, the available commercial colorimeters do not allow a global analysis over entire surfaces, since they measure $L^*a^*b^*$ coordinates only over a few square centimeters, coinciding with the dimension of the measurement area (around 10 mm). Thus, their measurements are not representative in heterogeneous materials such as food products (Papadakis et al., 2000; Mendoza and Aguilera, 2004). On the contrary, computer vision systems (CVSs) allow acquisition of digital images of entire samples that can be analyzed pixel by pixel, allowing accurate measurement of color coordinates in each point of the surface. Recently, León et al. (2006) demonstrated a computer vision system (CVS) for measuring color in $L^*a^*b^*$ coordinates from RGB space. Some studies have been undertaken to apply that approximation to food (Pedreschi et al., 2007; Quevedo et al., 2008). During the description of browning kinetics using color information, an L^* mean value is generally assumed. That is, an average of the L^* values is calculated using a CVS for an analyzed area. However, in apple slices, the development of non-uniform color patterns during browning (specifically L^* color) was observed. With the aim of quantifying non-homogenous color surfaces in apple slices during browning, Yoruk et al. (2004) employed an approximation, based on the reduction of the original number of red, green and blue intensity levels. They adopted a sub-color space derived from the RGB space, in which each color axis (Red, Green, Blue), normally ranging from 0 to 255, was divided by eight so that the colors were regrouped in $8 \times 8 \times 8 = 512$ ranges. Texture image analysis has been suggested as a possible tool to quantify color information extracted from both gray and color images without reducing the intensity levels of the RGB components. This has been possible because the texture of images is usually determined by analyzing the surface intensity obtained by plotting the (x, y) pixel coordinates *against* the gray level of each pixel (z axis). As a result, the changes in pixel value intensity reflect the texture of the image, which might contain information about the color and the geometric structure of the objects in the image (Quevedo et al., 2002; Du and Sun, 2004; Zheng et al., 2006; Gonzales-Barron and Butler, 2008). Until now, image texture analysis has been employed to quantify the non-homogenous distribution of the L^* color in fresh-cut products with a cubical shape (2 cm × 2 cm × 2 cm) (Quevedo et al., 2009a,b,c). The aim of this work was to classify fresh-cut apple slices on the basis of their browning state by employing a multispectral image vision system. The main objective was to identify proper virtual images as a combination of monochromatic ones in order to detect changes in color related to the browning process.

2. Materials and methods

2.1. Fruit samples

Apple fruit (*Malus domestica* Borkh. L. cultivar Granny Smith) from France (category: I; caliber: 80/85 mm) were purchased from a local wholesale produce distributor. Two sets of fifteen apples (*Set 1* and *Set 2*) were selected based on their regular shape and uniform size and they were employed as calibration and validation sets respectively. The apples were peeled and cut into eight equal slices in a refrigerated room at 7.5 °C and 85% RH, resulting in a total of 120 slices. After covering the slices with a cling film, they were stored at 7.5 °C for 9 days. A sharp stainless-steel knife was used throughout the process to reduce mechanical bruising. A single slice was considered to be a sample unit for these experiments. Twenty-four samples were evaluated at zero time and after storage for 1, 3, 7 and 9 days. In this experiment, each storage time corresponded to a treatment: zero time is the t_0 treatment, one day of storage is the t_1 treatment, three days of storage is the t_3 treatment and so on.

2.2. Reference values

Visible (VIS) relative reflectance spectra and CIE $L^*a^*b^*$ color coordinates were obtained from the samples using a Minolta CM-50I portable spectrophotometer (Konica Minolta Sensing, Inc., Japan), whose measurement area had a diameter of 8 mm. All measurements were taken under the conditions of standard illuminant D65 and 10° observer. A standard white calibration plate was employed to calibrate the equipment. Measurements were performed three times on each side of every apple slice, by positioning the measurement area in the center of the samples, which corresponded to the region where browning process was more clearly visible. An average VIS relative reflectance spectrum and a set of color coordinates expressed as average values were thus obtained for each apple slide. Browning of the cut surfaces from each sample was also evaluated visually according to a visual color scale. All analyses were carried out using MATLAB® software (MathWorks, Inc., USA).

2.2.1. Reflectance spectra analysis

Visible relative reflectance spectra 360–740 nm, at 10 nm intervals, were obtained from each sample and for each treatment. In order to simplify processing, reduce the dimension of the data and identify the most important features associated with the acquired spectra, a principal components analysis (PCA) was performed on the reflectance data after normalizing the spectra, which employed the *Total Absolute Sum* normalization, and after autoscaling spectra with the *Standard Normal Variate* (SNV) method (Barnes et al., 1993). The original number of variables K, corresponding to the thirty-nine wavelengths, could thus be reduced to a much smaller number (A) of variables called principal components (PCs), which were orthogonal linear combinations of the original 39 variables, and they accounted for most of the variability in the data. Moreover, the examination of loading plots generated by the PCA would identify the optical ranges related to the main differences between the different treatments. In order to decide how many components (and corresponding variants) to retain, the *scree test* (Otto, 2007) was applied, which is one of the most commonly used criteria. This criterion is based on the phenomenon of the residual variance leveling off when the proper number of PCs is obtained: after plotting the eigenvalues against the PCs in a scree plot, the component number can be derived from the leveling off in this dependence. Since the number of PCs can slightly vary depending on the test applied, the results obtained were tested with the *eigenvalue-one criterion:* according to this, only the PCs with eigenvalues greater than one could be significant in the analysis (Otto, 2007). Finally, a one-way ANOVA was performed on the PCs score values in order to test the ability of the *scree test* to capture the variability between the treatments. A test of mean comparisons according to Fisher's least significant difference (LSD) was applied, with a level of significance

of 0.05 was used to determine which means were significantly different.

2.2.2. Color parameters

CIE $L^*a^*b^*$ coordinates were measured, where L^* is the luminance component (ranging from 0 to 100), while a^* and b^* are color coordinates related respectively with the red/green and yellow/blue spectral ranges, with values varying from −120 to +120 (Yam and Papadakis, 2004). The results were also reported as *XYZ* tristimulus values. As such, it was possible to calculate the browning index (BI) by applying the equation defined by Buera et al. (1986) (1):

$$\mathrm{BI} = \frac{(x - 0.31)}{0.172} \times 100 \quad (1)$$

Variable x is the chromaticity coordinate calculated from the *XYZ* values according to the following formula $x = X/(X+Y+Z)$. The results were employed as a reference of browning during storage with regard to multispectral image information.

2.2.3. Sensory evaluation

Based on techniques from other studies investigating the relationship between changes in color of food products and their consumer evaluations (Abbott et al., 2004; Zhou et al., 2004; Perez-Gago et al., 2006; Pristijono et al., 2006; Quevedo et al., 2008), the shelf-life of each apple slice was determined as the time required for browning to develop to an unacceptable level. Browning of the cut surfaces was evaluated by three referees according to a visual color scale of 1–5, where 1 = fresh without any browning, 2 = slight browning of the cut surface, 3 = moderate browning, 4 = severe brown discoloration, 5 = complete discoloration. A sensory evaluation index (I_{SE}) was obtained for each sample by averaging the three scores of the sensory panel. This index was employed as a reference for the browning state of the samples and was compared to the information obtained from the vision system.

2.3. The vision system

Images were acquired through a multispectral imaging system consisting of a frame-grabber (National Instruments®, Austin, TX, USA) and a 3-CCD camera (DuncanTech/Redlake MS-3100®, Redlake Inc., USA) with a digital output. The camera resolution was 1300 × 1000 pixels with three band-pass filters (band-width: 20 nm) centered at 800 nm (infrared, IR), 680 nm (red, R), and 450 nm (blue, B). Acquired images were stored as 1300-by-1000-by-3 data arrays (IRRB images) that defined the infrared, red, and blue color components for each individual pixel. The light source was provided by six 100 W/220 V halogen lamps and the object distance between the lens system and the sample was 60 cm. The angle between the camera lens axis and the lighting source axis was 45° because the diffuse reflection responsible for the color occurs at 45° from the incident light (Francis and Clydesdale, 1975; Marcus and Kurt, 1998). The images were acquired using a black background. A black canvas was put around the vision test station in order to create a uniform light field around the object and to eliminate any effect of environmental light.

2.3.1. Image analysis: image segmentation and virtual images calculation

IRRB images were acquired for each sample and for each treatment and they were stored and processed off-line in MatLab®. At first, samples were distinguished from the background through the *Otsu method* (Otsu, 1979), a common segmentation technique. This technique computes the threshold level based on the image histogram distribution. It was performed on the IR images since they presented the greatest difference between the gray levels

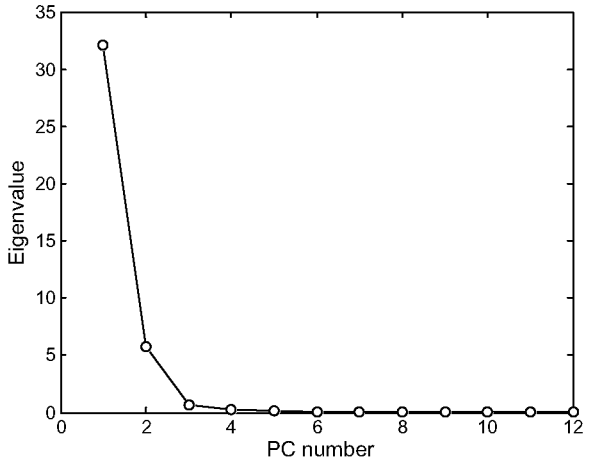

Fig. 1. Scree plot for the principal component model of the reflectance data. The *X* axis corresponds to the component number and the *Y* axis to the eigenvalues.

corresponding to samples (the region of interest, ROI) and to the background. This operation resulted in a binary image that could be considered as an "image mask" (gray level: ROI = 1 and background = 0). This mask was multiplied by the images acquired at 800 nm (IR), 680 nm (R) and 450 nm (B) and by a proper combination of monochromatic images (virtual images) to obtain the corresponding images only for the ROI. Further analyses were

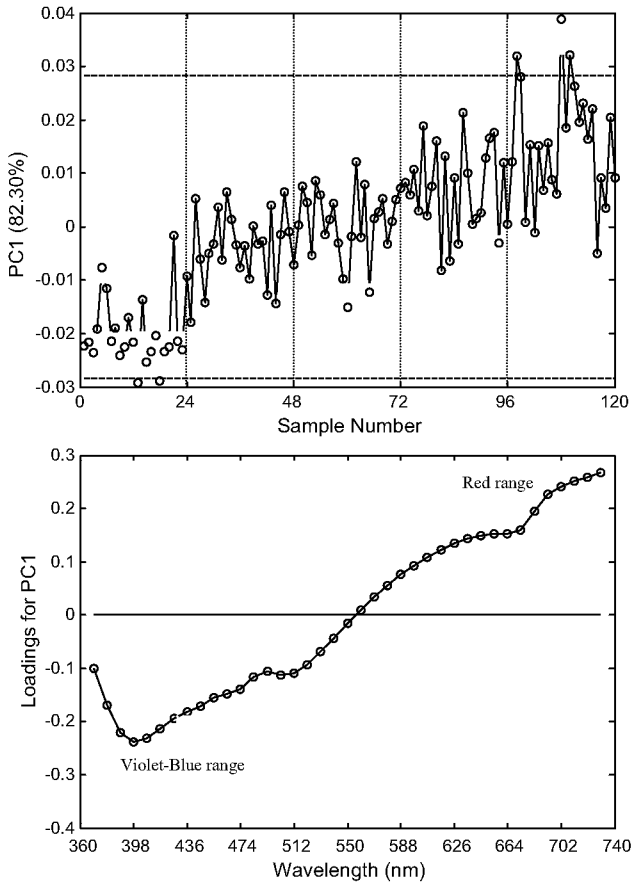

Fig. 2. Upper panel: PC1 scores plot for autoscaled and normalized reflectance data with 95% confidence limits (dotted lines). The *X* axis corresponds to the sample number and the *Y* axis to the sample scores for PC1. Vertical lines separate the samples based on treatment. Lower panel: PC1 loadings plot. The *X* axis corresponds to the wavelength (nm) and the *Y* axis to the loading values for PC1.

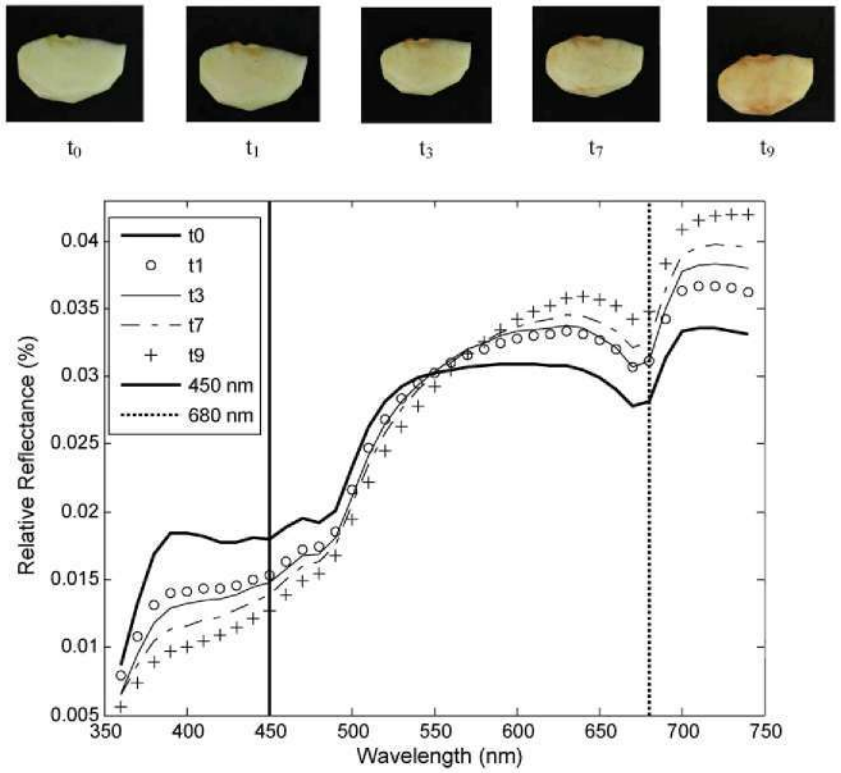

Fig. 3. The upper panel shows a fresh-cut apple slice at zero time (t_0) and after 1 (t_1), 3 (t_3), 7 (t_7) and 9 (t_9) days of storage ($T = 7.5$ °C). The lower panel shows the normalized (*Total Absolute Sum* normalization) VIS relative reflectance spectra acquired from the samples during the different treatments. Vertical lines indicate the blue (continuum line) and the red (dotted line) spectra regions according to the center of the B (450 nm) and of the R (680 nm) band-pass filters of the multispectral camera. The *X* axis corresponds to the wavelength (nm) and the *Y* axis to the VIS relative reflectance of the spectra (arbitrary units).

applied on the ROI-relative histograms of the virtual images, which were computed as the relative frequency of pixels over the intensity range of the image. In the rest of this document, "histogram" refers to "relative histogram" of the image.

2.3.2. Non-supervised image classification

A non-supervised classification according to Ward's method (Ward, 1963) was performed in order to define *browning reference classes* (BRC) based on the histograms of the virtual images of *Set 1* (calibration set). A multidimensional space was considered, where each dimension corresponded to an intensity level of the R − B/R + B, R − B and B/R histograms. Each histogram was thus represented as a single point on the multidimensional space. Ward's classification method was applied by computing the matrix of Euclidean distances between each pair of individuals (histograms), grouping the closest individuals and hierarchically merging groups (or individuals) whose combination gave the least *Ward linkage distance* (that is the minimum increase within the sum of squares of the new-formed group). As an advantage to other classification methods, Ward's method takes into account all histograms of the data set at every level of the grouping, producing very well structured and homogeneous groups (Otto, 2007). Besides, this method gave rise to successful results in previous works investigating fruit ripeness (Lleó et al., 2009; Herrero et al., 2011). A MatLab® devoted code was developed in order to generate groups automatically on the basis of the input maximum *Ward linkage distance*, which is derived from the analysis of the cluster tree features. The average histogram was computed for each generated group and defined as BRC.

2.3.3. Validation: classification of anonymous samples into browning reference classes

A validation procedure was developed to assess the errors in real time classification of anonymous images. Internal and external validations were successively carried out by assigning each anonymous individual into the previously generated BRC. Each anonymous histogram was classified into the reference class (each one defined by the average histogram of the class) to which it computed the minimum Euclidean classification distance.

For internal validation, the same population generating the model was classified again, one by one, into the BRC: the *observed* classification of the samples was compared with the *predicted* classification of the same samples, obtained by computing the Euclidean distances between the histogram of the samples image and the average histograms of the generated BRC.

In order to test the robustness of the model based on *Set 1* data, it was validated with *Set 2* samples and their corresponding histograms were classified into the BRC generated from *Set 1* data.

Table 1
The 12 first PCs resulting from the PCA performed with the autoscaled and normalized reflectance data.

Component number	Eigenvalue	Percent of variance	Cumulative percentage
1	32.0973	82.301	82.30
2	5.7639	14.779	97.08
3	0.6424	1.647	98.72
4	0.2921	0.749	99.47
5	0.1026	0.263	99.74
6	0.0621	0.159	99.89
7	0.0206	0.053	99.95
8	0.0065	0.017	99.96
9	0.0043	0.011	99.98
10	0.0022	0.006	99.98
11	0.0015	0.004	99.99
12	0.0011	0.003	99.99

2.4. Statistical analysis of reference values

Color reference parameters (CIE $L^*a^*b^*$ coordinates and BI) and I_{SE} were compared to the classification based on the histograms of virtual images of each index. An ANOVA was performed on L^*, a^*, b^*, BI and I_{SE} values and on the clusters extracted from the image analysis. A mean comparison procedure (LSD test) was applied, with a level of significance of 0.05. Statistical procedures were performed using MatLab 7.0® and STATGRAPHICS Plus 5.1 (Manugistics Inc., Rockville, MD, USA).

3. Results and discussion

3.1. PCA of reflectance spectra

In the scree plot reported in Fig. 1, the slope changes between the second and third components. Therefore, according to the *scree test*, two significant PCs were revealed. The same result was obtained through the *eigenvalue-one criterion*, since only the eigenvalues of PC1 and PC2 were greater than one (Table 1). The percent variance captured by the PC1 and PC2 explained 97.08% of the variability in the data set (Table 1). In the plot of PC1 scores against sample number ($n = 120$) (Fig. 2), it was possible to observe that the lowest PC1 scores corresponded to the samples submitted to the t_0 treatment (1–24), whereas the samples corresponding to the t_9 treatment were characterized by the higher scores (96–120). Besides, PC1 scores of samples submitted to the t_1 (25–48), t_3 (49–71) and t_7 (72–95) treatments were in between the t_0 and t_9 values and increased over time. On the contrary, in the plot of PC2, PC3 and PC4 scores (not shown) against sample number, no consistent trends were found, suggesting that the variability of these components, which accounted for 14.78%, 1.65% and 0.76% respectively of the total variance (Table 1), was not related to the treatments. The above considerations suggested that the variability associated with PC1, which accounted for 82.30% of the total variance, could explain the difference between the samples analyzed at zero time and after storage for 1, 3, 7 and 9 days. Since PC1 yielded highly negative loadings in the 380–440 nm range (corresponding to the violet-blue zone) and highly positive loadings in the 670–740 nm range (red region) (Fig. 2), these wavelengths were related to the variability between the different treatments. From the ANOVA performed on the PC1 scores, there was a significant difference between the scores and the different treatments ($F = 64.3$, $\alpha = 0.05$) (Table 2). After performing the LSD test, five homogenous groups were identified (data not shown). This means that the proposed method was able to select proper subsets of wavelengths in which the variability was associated with the treatments. This suggested that the 360–490 nm and 620–700 spectral ranges had the closest relationship to changes in pigment content during the browning process. Fig. 3 shows the VIS reflectance spectra after applying the *Total Absolute Sum* normalization of a fresh-cut apple slice at zero time (t_0) and of the same sample after treatments t_0, t_1, t_3, t_7 and t_9. The shape of these spectra confirmed the results obtained from the PCA. The main difference is that the relative reflectance values in the blue (430–490 nm) area are higher at the beginning of the storage period than at the end, whereas the reflectance values in the red (620–700 nm) ranges are lower at t_0 than at t_9. This agrees with previous studies that have observed that an increase in enzymatic browning in fresh-cut products during storage is accompanied by an increase in colorimetric a^* and b^* values (Pristijono et al., 2006; Lu et al., 2007). This means that during the enzymatic browning, apple surface color changes to red and yellow. The increase of red and yellow color components could explain the increase in pinkish-red colors in apple slices over time. The appearance of pinkish-red off-colored compounds has been attributed to phenol regeneration during the

Table 2
An ANOVA table for PC1 organized by treatment.

Source	Sum of squares	D.f.	Mean square	F	P-Value
Between groups	2644.98	4	661.24	64.74	0.0000
Within groups	1174.60	115	10.21		
Total (Corr.)	3819.58	119			

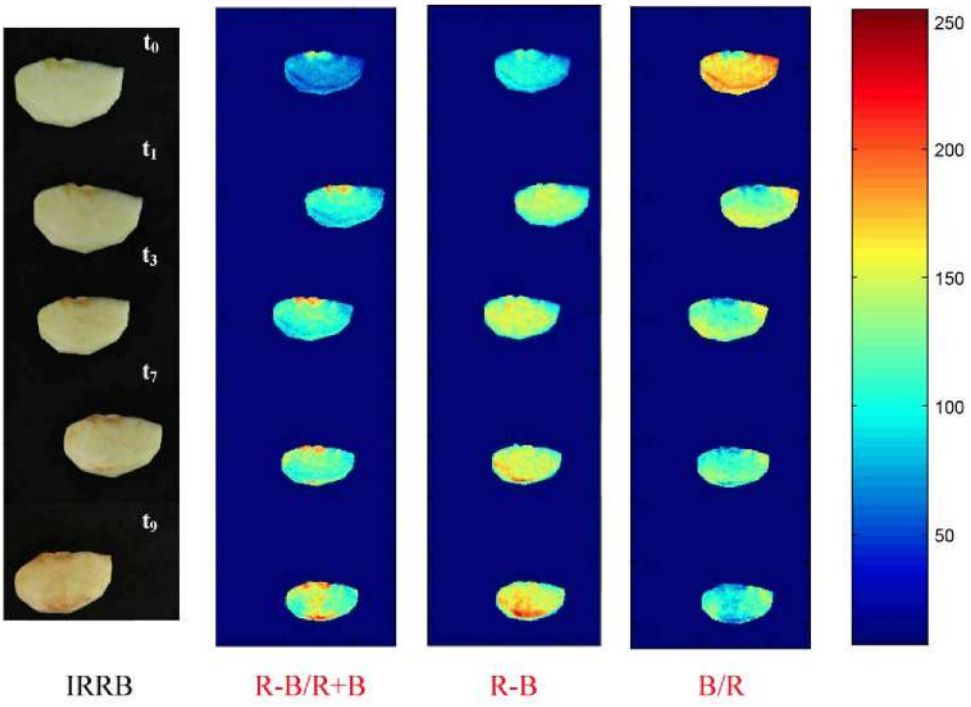

Fig. 4. IRRB image and R − B/R + B, R − B, B/R virtual images of an apple slice sample computed at zero time (t_0) and after storage for 1, 3, 7 and 9 days (t_1, t_3, t_7 and t_9). The color scale represents the intensity values of the images.

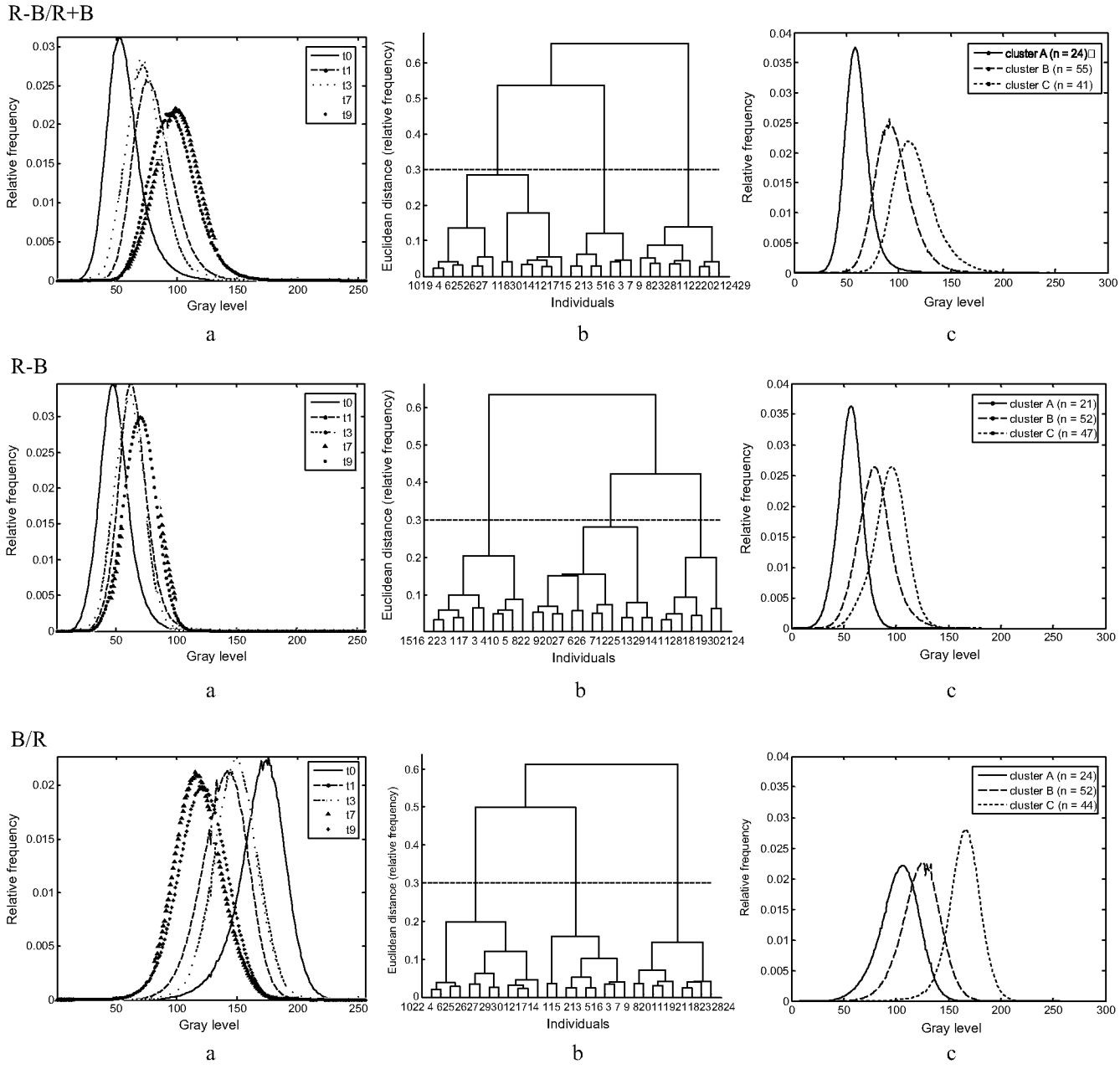

Fig. 5. (a) plots the average histograms calculated from the samples for each image based class (R – B/R + B, R – B and B/R) and for each treatment (t_0, t_1, t_3, t_7 and t_9); (b) reports the relative dendrograms generated by applying Ward's non-supervised classification and (c) shows the average histograms computed for each generated cluster and defined as browning reference class (BRC). Horizontal lines in the cluster trees represent the maximum Ward Linkage distance within groups (pixel relative frequency = 0.30).

oxidation process with deep color formation (Richard-Forget et al., 1991).

3.2. Virtual images

On the basis of the results obtained from the analysis of VIS spectra, proper virtual images were calculated as a combination of red and blue images of the samples acquired by the IRRB camera. Since the reflectance values corresponding to the red range increased from t_0 to t_9, whereas those corresponding to the blue region decreased, the virtual images were calculated to amplify these differences. The following virtual images were computed: (R – B)/(R + B), R – B and B/R. In the rest of this paper, R – B/R + B refers to (R – B)/(R + B). Fig. 4 shows an example of these virtual images for one sample in each treatment. In all cases, from t_0 to t_9 treatment, changes in color were observed in the samples, which corresponded to a change in pixel intensity values. In R – B/R + B and R – B images, the pixel intensity values increased during the storage period. In the B/R images, the pixel intensity value decreased. These changes in color did not occur uniformly in the analyzed samples since the same samples presented regions whose pixels turned to higher (or lower) intensity values faster than others. This could be related to the increase in enzymatic activity, which results from tissue disruption and takes place at a different rate on the cut surface according to the local substrate composition and to the amount of enzymes *that initiated the browning* (Li-Qin et al., 2009). By comparing virtual images with the original samples (Fig. 4), the sub-regions corresponding to the zones of the surface whose color turned brown during storage could be identified.

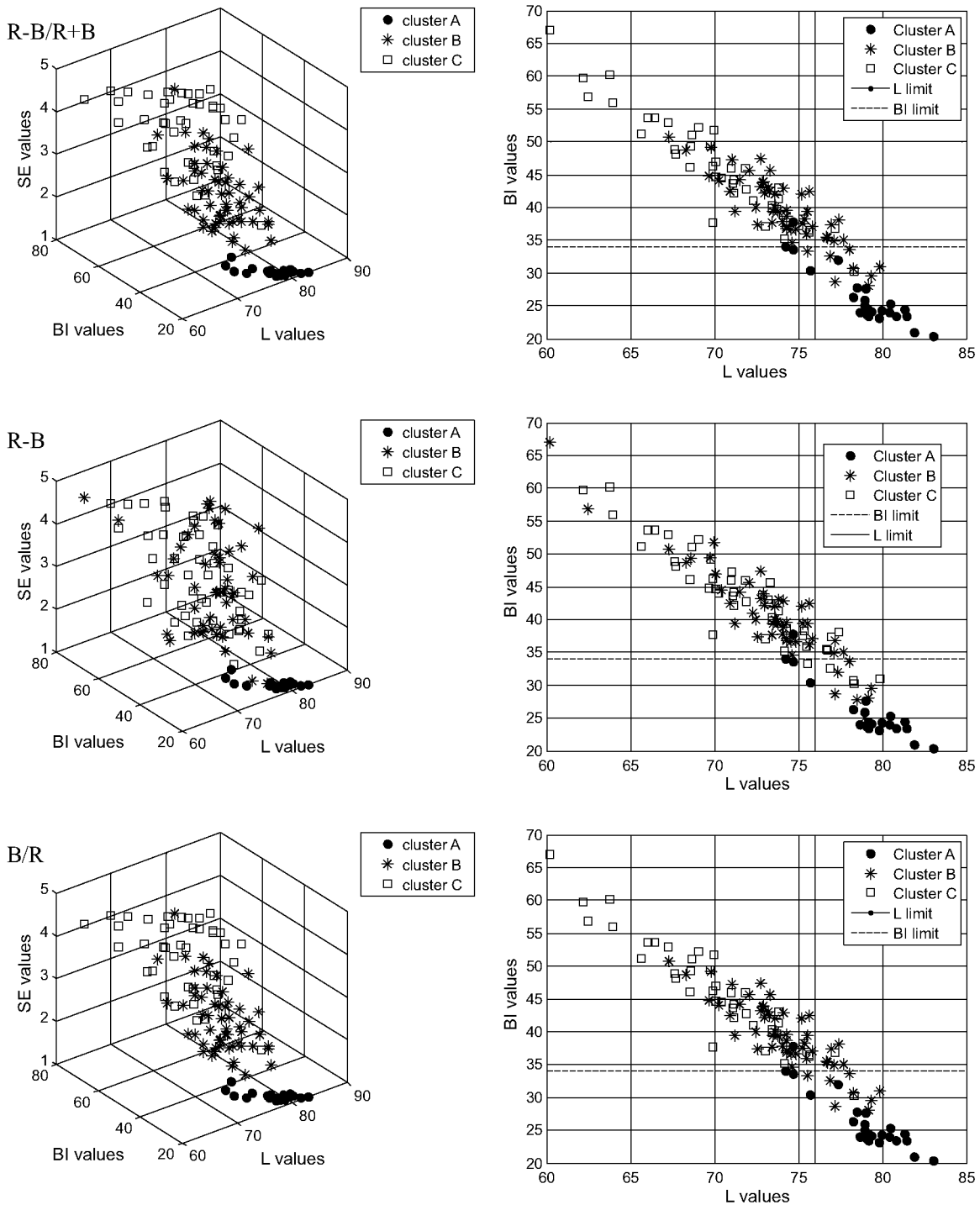

Fig. 6. 3-D plots (left column) of L, BI and I_{SE} index values and bi-plots of BI against L values (right column) of *Set 1* samples categorized in their corresponding image-based cluster (A–C) obtained from R – B/R + B, R – B and B/R image histograms (Ward's method). In the bi-plots of the right column, the vertical and horizontal lines represent the L_{limit} (76.0) and the BI_{limit} values (34.07), respectively.

3.3. Generation of browning reference classes

For each virtual image (*i.e.*, R – B/R + B, R – B and B/R) the average of the twenty-four ROI-histograms obtained during each one of the treatments t_0, t_1, t_3, t_7 and t_9 was calculated, obtaining five average histograms per image combination (Fig. 5). The average histograms of R – B/R + B and R – B images shifted to higher intensity values, while those of B/R images shifted to lower intensity values. Fig. 5 also shows the dendrograms that were generated by applying Ward's non-supervised classification to each virtual image. On the basis of the dendrogram features, the maximum *Ward linkage distance* within groups was set at a 0.30 pixel relative frequency. In all cases, three clusters, corresponding to the three BRC (Cluster A, Cluster B and Cluster C) were obtained. In the same figure, the average histograms computed for each generated cluster and defined as BRC are also shown. Regarding the population classified in the different clusters, R – B/R + B and B/R images generated clusters that were highly related to the various treatments:

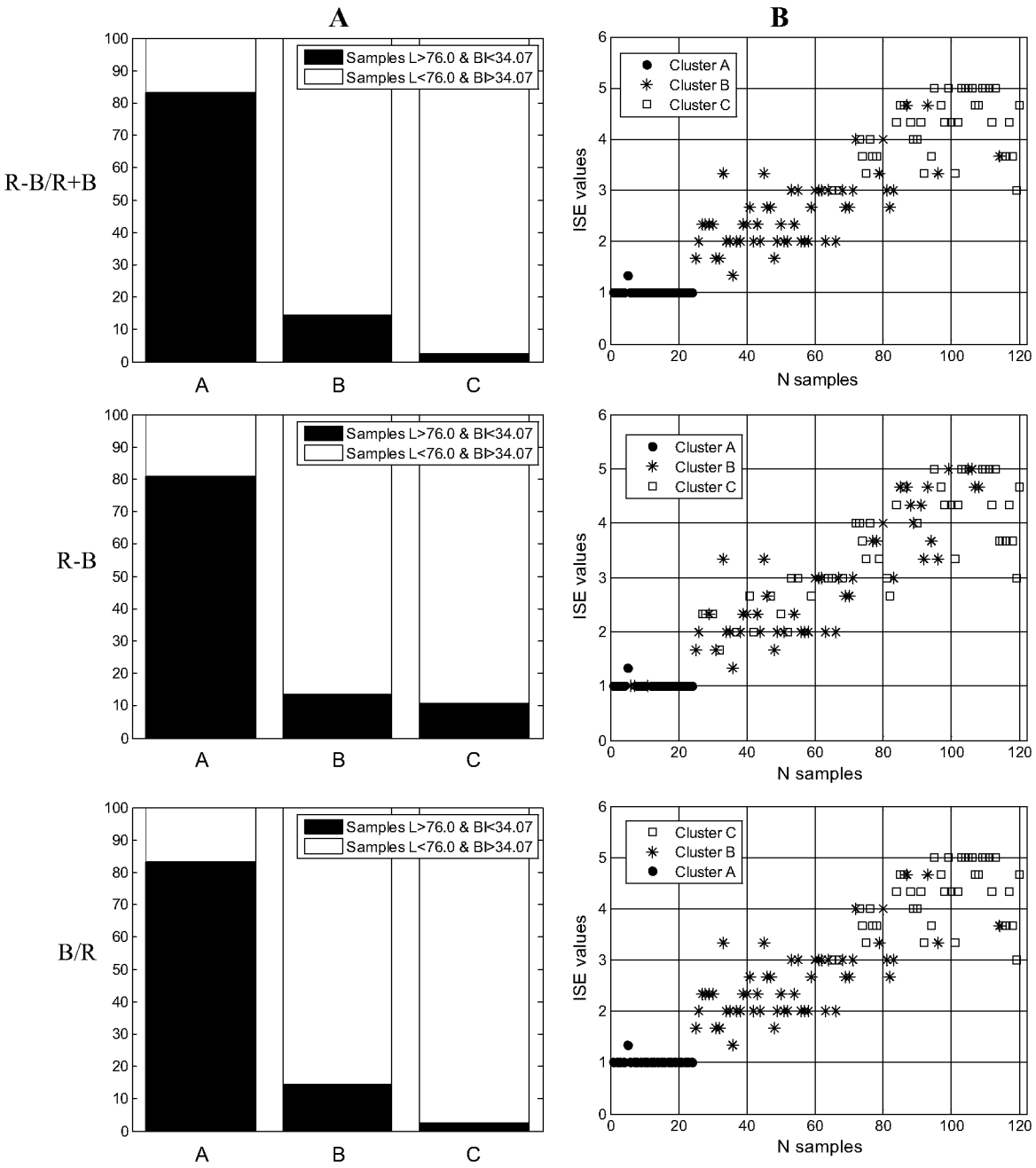

Fig. 7. Stacked bar plots (left column) obtained by selecting samples with L^* values >76 and BI values <34.07 for each cluster (the *X* axis corresponds to the A, B and C Clusters and the *Y* axis to the sample percentage for each range) and plots of I_{SE} values against sample number, where samples are categorized in their corresponding image-based cluster.

100% of Cluster A consisted of samples analyzed at zero time, nearly 85% of Cluster B was composed of samples belonging to the t_1 and t_3 treatments and nearly 95% of Cluster C were samples that were part of to the t_7 and t_9 treatments. The classification based on R – B images was less related to the treatments (Cluster A: 95% of t_0 and 5% of t_1; Cluster B: 60% of t_1 and t_3, 38% of t_7 and t_9, 2% of t_0; Cluster C: 60% of t_7 and t_9, 40% of t_1 and t_3).

3.4. Internal validation

Internal validation of the model showed that in the case of the R – B/R + B and B/R histograms, 99.2% of the samples were classified in the same group by two methods: the Ward's non-supervised classification (BRC from A to C) and the classification according to Euclidean distances to Ward-generated reference classes. For R – B histograms, nearly 96% of the samples were classified in the same group by both methods (table not shown).

3.5. External validation

The proposed classifications showed satisfactory results after testing for their robustness. The classification of anonymous histograms of *Set 2* samples, obtained by calculating the minimum E_d distance to the reference classes generated with R – B/R + B, R – B and B/R histograms of *Set 1* samples was able to correctly classify 84, 66 and 81%, respectively, of the samples considered from *Set 2* (table not shown).

Table 3
Average values, confidence intervals (95%) and the results of an ANOVA Fisher LSD test performed on L^*, a^*, b^*, BI and I_{SE} values. The values come from samples grouped in Clusters A–C according to Ward's method based on R – B/R + B, R – B and B/R image histograms. An asterisk indicates that there is a significant difference ($P < 0.05$) between all of the means.

		Reference values									
	Cluster	L^* mean	$\pm 1.96SD_{L^*}$	a^* mean	$\pm 1.96SD_{a^*}$	b^* mean	$\pm 1.96SD_{b^*}$	BI* mean	$\pm 1.96SD_{BI}$	I_{SE}* mean	$\pm 1.96SD_{SE}$
R – B/R + B	A	78.92	0.65	−1.28	0.30	21.28	0.65	21.28	0.67	1.00	0.13
	B	74.35	0.41	1.52	0.25	28.60	0.44	28.60	0.44	2.57	0.07
	C	70.21	0.49	3.55	0.22	30.80	0.52	30.85	0.51	4.20	0.08
	F-values	59.58*		77.21*		65.80*		81.71*		211.21*	
R – B	A	79.05	0.63	−1.31	0.37	21.10	0.78	25.96	1.57	1.01	0.21
	B	73.46	0.42	1.76	0.24	29.04	0.49	40.42	0.97	2.89	0.13
	C	71.77	0.50	2.98	0.25	29.69	0.52	43.29	1.02	3.57	0.14
	F-values	28.23*		44.30*		45.85*		46.33*		49.62*	
B/R	A	78.95	0.64	−1.24	0.31	21.28	0.67	26.25	1.23	1.01	0.12
	B	74.25	0.42	1.59	0.20	28.61	0.44	39.27	0.81	2.58	0.08
	C	70.11	0.49	3.58	0.24	30.85	0.51	46.13	0.94	4.22	0.09
	F-values	59.60*		77.25*		65.96*		81.72*		210.76*	

3.6. Reference parameters of image based clusters

Table 3 reports the results of an ANOVA performed on L^*, a^*, b^*, BI and I_{SE} values as well as the clusters obtained through the described non-supervised classification of the image histograms. For each index and for each image-based cluster, a consistent increase was observed in a^*, b^*, BI and I_{SE} values as well as a consistent decrease in lightness (L^*) from Clusters A to C. The trend of these parameters agreed with the results of previous studies that examined the changes in color coordinates related to enzymatic browning from storage (Perez-Gago et al., 2006; Pristijono et al., 2006; Lu et al., 2007; Toivonen, 2008). After performing the LSD test, significant differences were observed between all the means of the analyzed variables. In other words, Clusters A–C could be considered homogenous in regards to color parameters and to sensory evaluation. The left column of Fig. 6 provides 3-D plots of L^*, BI and I_{SE} values of *Set 1* samples categorized in their corresponding image-based cluster (A–C). The relationship between BI values and L^* values was analyzed and the linear model reported in Eq. (2) was obtained:

$$BI = \beta_0 + \beta_1(L*) \quad (2)$$

where $\beta_0 = 184.25$, $\beta_1 = -197$ and $R^2 = 90.1\%$. According to the results obtained by Pristijono et al. (2006) in a study investigating browning in 'Granny Smith' apple slices, an L^* value of 76.0 was considered to be the limit for acceptability of browning ($L_{limit} = 76$). Eq. (2) allowed us to predict the threshold value for BI (BI_{limit}) corresponding to L_{limit} and we found that $BI_{limit} = 34.07$. This value was considered to be a threshold value for browning with a 95% confidence interval. These limits are reported in the bi-plots of BI against L^* values showed in the right column of Fig. 6. Considering L_{limit} and BI_{limit} limits, Cluster A, B and C samples were classified in slices with acceptable ($L > 76$ and $BI < 34.07$) and inacceptable browning ($L < 76$ and $BI > 34.07$) (left column of Fig. 7). According to these classifications, nearly 84% of Cluster A, 15% of Cluster B and 2% of Cluster C (calculated with R – B/R + B and B/R images) and nearly 80% of Cluster A, 13% of Cluster B and 10% of Cluster C (calculated with R – B images) were considered to have acceptable levels of browning. According to sensory evaluation, which considered a color scale of 1–5 for each sample, all Cluster A samples were judged as *fresh without any browning*, while almost all Cluster B and Cluster C samples were evaluated as samples with *slight-moderate* and *severe-complete browning of the cut surface*, respectively (right column of Fig. 7). These results suggested that the proposed vision system was able to classify samples according to colorimetric and sensory parameters since Cluster A would mainly comprise samples with a cut surface without browning, while Cluster B and C samples would exhibit different degrees of browning. Considering the three image-based classifications, R – B/R + B and B/R images showed the best agreement between treatments submitted to the sample, color parameters and I_{SE} values. On the basis of these results, image-based classes may provide relevant information for the management of fresh-cut apple slices and has the potential to help detect fruit with an unacceptable level of browning.

4. Conclusions

In the present study, a new method based on a multispectral vision system was proposed to classify fresh-cut apple slices according to enzymatic browning evolution. The method utilized relative histograms of virtual images, *i.e.*, R – B/R + B R – B and B/R, as well as combinations of red (R, 680 nm) and blue (B, 450 nm) images of the samples. The red and blue spectral ranges contained enough information for the proposed method to adequately classify sample images. On the basis of our internal classification results, all the indexes were sufficient to detect changes in browning by classifying the samples into three reference classes (A–C). In all cases, Clusters A–C presented decreasing lightness and increasing a^*, b^*, BI and I_{SE} values. The robustness of the classification procedure was determined by applying an external validation to a second set of samples. It was possible to correctly classify a high percentage of images from fruit in the second testing set with the model generated with the first set. The classification based on R – B/R + B and B/R images exhibited the best sensitivity for reflecting the change in colors associated with browning. All these results confirmed the potential of the proposed method for characterizing fresh-cut apples according to their browning state. This method could be used as a potential criterion for establishing the optimal shelf-life of fresh-cut apple slices under refrigeration conditions with or without additional inhibitory treatments. In addition, this method allows for a more spatially detailed determination compared to other colorimetric techniques, which analyze a small portion of a sample and lead to errors and inaccurate results if the analysis is not repeated in different zones on the surface. Moreover, colorimetric measurements can only be made if there is contact with the surface of the fruit and cannot be automated. On the contrary, analyzing the histogram for the whole image of each sample is an easier and faster technique that allows quantification based on the original colors of the sample.

Acknowledgements

This research was carried out in the *Universidad Politécnica de Madrid* (Spain) and was supported by the project MULTIHORT, funded by the Spanish *Ministerio de Ciencia e Innovación*

(MCINN), and by the European project ISAFRUIT (FP6 FOOD 016279-2).

References

Abbott, J.A., Saftner, R.A., Gross, K.C., Vinyard, B.T., Janick, J., 2004. Consumer evaluation and quality measurement of fresh-cut slices of Fuji, Golden Delicious, GoldRush, and Granny Smith apples. Postharvest Biol. Technol. 33, 127–140.

Baldwin, E.A., Nisperos, M.O., Chen, X., Hagenmaier, R.D., 1996. Improving storage life of cut apple and potato with edible coating. Postharvest Biol. Technol. 9, 151–163.

Barnes, R.J., Dhanoa, M.S., Lister, S.J., 1993. Correction to the description of standard normal variate (snv) and de-trend transformations in practical spectroscopy with applications in food and beverage analysis – 2nd edition. J. Near Infrared Spec. 1, 185–186.

Buera, M.P., Lozano, R.D., Petriella, C., 1986. Definition of colour in the non enzymatic browning process. Die. Farbe 32, 318–322.

Du, C.-J., Sun, D.-W., 2004. Recent developments in the applications of image processing techniques for food quality evaluation. Trends Food Sci. Technol. 15, 230–249.

Francis, F.J., Clydesdale, F.M., 1975. Food Colorimetry: Theory and Applications. AVI Publ. Co., Westport.

Gonzales-Barron, U., Butler, F., 2008. Discrimination of crumb grain visual appearance of organic and non-organic bread loaves by image texture analysis. J. Food Eng. 84, 480–488.

Herrero, A., Lunadei, L., Lleó, L., Diezma, B.M.R., 2011. Multispectral vision for monitoring fruit ripeness. J. Food Sci., doi:10.1111/j.1750-3841.2010.02000.x, in press.

Hosoda, H., Inoue, E., Iwahashi, Y., Sakaue, K., Tada, M., Nagata, T., 2005. Inhibitory effect of sulfides on browning of apple slice. J. Jap. Soc. Food Sci. Technol. 52, 120–124.

Kang, K.J., Oh, G.S., Go, Y.S., Kim, Y.J., Park, D.H., Kim, H.Y., 2004. Inhibition of enzymatic browning in Paeoniae radix rubra by citric acid. Food Sci. Biotechnol. 13, 119–125.

Lambrecht, H.S., 1995. Sulfite substitutes for the prevention of enzymatic browning in foods. Enzymatic Browning Prev., 313–323.

León, K., Mery, D., Pedreschi, F., León, J., 2006. Color measurement in L*a*b* units from RGB digital images. Food Res. Intl. 39, 1084–1091.

Li-Qin, Z., Jie, Z., Shu-Hua, Z., Lai-Hui, G., 2009. Inhibition of browning on the surface of peach slices by short-term exposure to nitric oxide and ascorbic acid. Food Chem. 114, 174–179.

Lleó, L., Barreiro, P., Ruiz-Altisent, M., Herrero, A., 2009. Multispectral images of peach related to firmness and maturity at harvest. J. Food Eng. 93, 229–235.

Lu, S., Luo, Y., Turner, E., Feng, H., 2007. Efficacy of sodium chlorite as an inhibitor of enzymatic browning in apple slices. Food Chem. 104, 824–829.

Marcus, R.T., Kurt, N., 1998. The Measurement of Color. Azimuth, North-Holland, pp. 31–96 (Chapter 2).

Mendoza, F., Aguilera, J.M., 2004. Application of image analysis for classification of ripening bananas. J. Food Sci. 69, E471–E477.

Osanai, Y., Motomura, Y., Sakurai, N., 2003. Effect of methyl bromide on the internal browning, firmness and elasticity of flesh in un-bagged apple 'Fuji' fruit. J. Jap. Soc. Food Sci. Technol. 50 (5), 254–258.

Otsu, N., 1979. A threshold selection method from gray-level histograms. IEEE Trans. Sys. Man. Cyber 9, 62–66.

Otto, M., 2007. Statistics and Computer Application in Analytical Chemistry, 2nd ed, Chichester.

Papadakis, S.E., Malek, S.A., Emery, R.E., Yam, K.L., 2000. A versatile and inexpensive technique for measuring color of foods. Food Technol. 54, 48–51.

Pedreschi, F., Bustos, O., Mery, D., Moyano, P., Kaack, K., Granby, K., 2007. Color kinetics and acrylamide formation in NaCl soaked potato chips. J. Food Eng. 79, 989–997.

Perez-Gago, M.B., Serra, M., Río, M.A.D., 2006. Color change of fresh-cut apples coated with whey protein concentrate-based edible coatings. Postharvest Biol. Technol. 39, 84–92.

Pristijono, P., Wills, R.B.H., Golding, J.B., 2006. Inhibition of browning on the surface of apple slices by short term exposure to nitric oxide (NO) gas. Postharvest Biol. Technol. 42, 256–259.

Quevedo, R., Aguilera, J.M., Pedreschi, F., 2008. Color of salmon fillets by computer vision and sensory panel. Food Bioprocess Technol., doi:10.1007/s11947-008-0106-6.

Quevedo, R., Carlos, L.-G., Aguilera, J.M., Cadoche, L., 2002. Description of food surfaces and microstructural changes using fractal image texture analysis. J. Food Eng. 53, 361–371.

Quevedo, R., Díaz, O., Caqueo, A., Ronceros, B., Aguilera, J.M., 2009a. Quantification of enzymatic browning kinetics in pear slices using non-homogenous L* color information from digital images. Food Sci. Technol. 42, 1367–1373.

Quevedo, R., Díaz, O., Ronceros, B., Pedreschi, F., Aguilera, J.M., 2009b. Description of the kinetic enzymatic browning in banana (*Musa cavendish*) slices using non-uniform color information from digital images. Food Res. Intl. 42, 1309–1314.

Quevedo, R., Jaramillo, M., Díaz, O., Pedreschi, F., Aguilera, J.M., 2009c. Quantification of enzymatic browning in apple slices applying the fractal texture Fourier image. J. Food Eng. 95, 285–290.

Richard-Forget, F.C., Goupy, P.M., Nicolas, J.J., Lacombe, J.M., Pavia, A.A., 1991. Cysteine as an inhibitor of enzymatic browning. 2. Kinetics studies. J. Agric. Food Chem. 39, 841–847.

Robards, K., Prenzler, P.D., Tucker, G., Swatsitang, P., Glover, W., 1999. Phenolic compounds and their role in oxidative processes in fruits. Food Chem. 66, 401–436.

Toivonen, P.M.A., 2008. Influence of harvest maturity on cut-edge browning of Granny Smith fresh apple slices treated with anti-browning solution after cutting. LWT-Food Sci. Technol. 41, 1607–1609.

Ward Jr., J.H., 1963. Hierarchical grouping to optimize an objective function. J. Am. Stat. Assoc. 58, 236–244.

Yam, K.L., Papadakis, S.E., 2004. A simple digital imaging method for measuring and analyzing color of food surfaces. J. Food Eng. 61, 137–142.

Yoruk, R., Yoruk, S., Balaban, M.O., Marshall, M.R., 2004. Machine vision analysis of antibrowning potency for oxalic acid: a comparative investigation on banana and apple. J. Food Sci. Technol. (Mysore) 69, E281–E289.

Zheng, C., Sun, D.-W., Zheng, L., 2006. Recent applications of image texture for evaluation of food qualities—a review. Trends Food Sci. Technol. 17, 113–128.

Zhou, T., Harrison, A.D., McKellar, R., Young, J.C., Odumeru, J., Piyasena, P., Lu, X., Mercer, D.G., Karr, S., 2004. Determination of acceptability and shelf life of ready-to-use lettuce by digital image analysis. Food Res. Intl. 37, 875–881.